Journal of Power Sources 196 (2011) 8041–8047

Contents lists available at ScienceDirect

Journal of Power Sources

journal homepage: www.elsevier.com/locate/jpowsour

Electrophoretic deposition of $(Mn,Co)_3O_4$ spinel coating for solid oxide fuel cell interconnects

Hui Zhang[a], Zhaolin Zhan[a,b], Xingbo Liu[a,*]

[a] Mechanical and Aerospace Engineering Department, West Virginia University, Morgantown, WV 26506, USA
[b] Kuming University of Science and Technology, Kunming 650093, PR China

ARTICLE INFO

Article history:
Received 18 March 2011
Received in revised form 13 May 2011
Accepted 19 May 2011
Available online 27 May 2011

Keywords:
Solid oxide fuel cell
Interconnect
Electrophoretic deposition
$(Mn,Co)_3O_4$ spinel

ABSTRACT

We discuss here our attempt to develop $(Mn,Co)_3O_4$ spinel coatings on the surface of Cr-containing steel through electrophoretic deposition (EPD) followed by reduced-atmosphere sintering for solid oxide fuel cell (SOFC) interconnect application. The effects of EPD voltages and sintering atmospheres on the microstructure, electrical conductivity and long-term stability of the coated interconnects are examined by means of scanning electron microscopy (SEM), energy dispersion spectrometry (EDS), X-ray photoelectron spectroscopy (XPS), and four-probe resistance techniques. For the spinel coatings generated using smaller voltage than 400 V, the interconnect surfaces exhibit good packing behavior and high conductivity. The reduced atmosphere during sintering has a beneficial impact on the minimizing chromia subscale formation and thus reducing the area specific resistance (ASR) of the coated interconnects. Moreover, it is interesting to note that a more stable long-term performance is achieved for the spinel coating sintered in H_2/H_2O atmosphere with thin chromia sub-scale and no Cr penetration. Based on the current results, EPD followed by reduced-atmosphere sintering is a fast and economic way to deposit $(Mn,Co)_3O_4$ coating for SOFC interconnect applications.

1. Introduction

Solid oxide fuel cells (SOFCs) are promising candidates for future energy conversion systems because they have higher energy conversion efficiency than conventional heat engine systems and other types of fuel cells. Among the four components in SOFC, i.e. anode, cathode, electrolyte, and interconnect, the material requirements for the interconnect are the most demanding because of its unique exposure conditions including complex gas phase chemistry, glass bonded or compressive seals, inhomogeneous temperature distribution, and thermal cycling [1–3]. Cr-containing stainless steels [4,5] have been widely used as metallic interconnects as a result of their electrically conducting oxide scale, good mechanical properties, appropriate thermal expansion behavior, very low cost and excellent manufacturability. However, there are two major issues associated with the use of these stainless steels. One is the evaporation and migration of Cr species from the chromia scale resulted from the presence of water vapor, another is electrical resistance increase over time due to continuous oxidation at elevated temperatures. These problems have deleterious impacts on contact resistance and long-term cell performance. A highly attractive solution is to deposit a protective layer on the surface of the steel interconnect.

Many efforts [6–10] have suggested that Mn–Co oxides are the most promising coating materials for protecting the steel interconnects and improving SOFCs' operation. For example, Kurokawa et al. [11] reported that $MnCo_2O_4$ coatings on Cr-containing stainless steels decreased chromium vaporization by a factor up to ~40 at 800 °C. Yang et al. [12] evaluated that $(Mn,Co)_3O_4$ spinel coatings were effective in reducing contact resistance and providing high electrical conductivity. In addition, our previous studies [13] indicated that the Cr diffusion was obviously suppressed and the degradation rate of SOFCs was significantly dropped by using Mn–Co oxide coatings. Although various Mn–Co oxide coatings, especially $(Mn,Co)_3O_4$ spinel coatings with high electrical conductivity, have shown great usability for SOFC interconnects, the growth of chromia layer is still inevitable at the substrate/coating interface. Such sub-coating oxide scale growth would lead to the increase of the area specific resistance (ASR) with time. It is therefore necessary to find a better approach to modify the interface performance and improve the long-term stability for SOFC application.

In this work, electrophoretic deposition (EPD) [14,15] followed by reduced-atmosphere sintering is employed in order to produce the desired $(Mn,Co)_3O_4$ spinel coatings on SOFC interconnects. As an alternative deposition process, EPD offers great advantages

* Corresponding author at: Department of Mechanical and Aerospace Engineering, West Virginia University, P.O. Box 6106, Morgantown, WV 26506, USA. Tel.: +1 304 293 3339; fax: +1 304 293 6689.
E-mail address: xingbo.liu@mail.wvu.edu (X. Liu).

0378-7753/$ – see front matter © 2011 Elsevier B.V. All rights reserved.
doi:10.1016/j.jpowsour.2011.05.053

in deposition efficiency, cost-effectiveness and ease of operation, as compared with other coating methods. Moreover, it is easy to obtain the desired $(Mn,Co)_3O_4$ spinel phase and control the coating thickness through direct application of $(Mn,Co)_3O_4$ particles and simple adjustment of process parameters. The strategy of subsequent sintering in reduced atmosphere is also determined by the intention to protect against Cr outward diffusion from metal substrate. Consequently, the main aim of this study is to examine the influence of reduced-atmosphere sintering on the growth of subcoating oxide scale and long-term ASR of SOFC interconnects. Also, the surface evolution and conductivity changes are investigated to evaluate the effect of EPD voltages under applied electric field.

2. Experimental

$(Mn,Co)_3O_4$ spinel powder was supplied from Praxair Co. (99.9%) with an average particle size of 0.9 μm. T441 steels (Allegheny Ludlum) were used as metallic substrate as well as counter electrode. They were cut into 50 mm × 10 mm coupons, polished with 600 grit sandpaper, cleaned in an ultrasonic acetone bath and then rinsed in ethanol. For an EPD process, the $(Mn,Co)_3O_4$ spinel powders were first dispersed in ethanol by ultrasonication for 3 h, to provide 5 wt% suspension. Then the electrodes were immersed into the suspension and a dc voltage was given for 1 min by a high voltage power source (Lambpa, USA). Finally, positively charged $(Mn,Co)_3O_4$ spinel particles were drifted and deposited on the T441 steel cathode.

Different voltages ranging from 200 to 500 V were used for obtaining high-performance $(Mn,Co)_3O_4$ spinel coatings. After deposition, the $(Mn,Co)_3O_4$ spinel layers were thermally treated at 800 °C for 2 h in air or H_2/H_2O (97% H_2–3% H_2O) atmospheres. All the heat treatment experiments were conducted with the heating and cooling rates of 5 °C min^{-1} to form stable protection coatings on T441 steels.

A field emission scanning electronic microscope (FESEM, JEOL 7600F) was used to observe the surface morphology of the protection layers at an acceleration voltage of 30 kV. The X-ray photoelectron spectroscopy (XPS) was performed on a Physical Electronics VersaProbe 5000 spectrometer with Al Kα radiation (1486.71 eV), and the binding energy scale was calibrated by C 1s peak at 284.8 eV. The morphologies of cross-section and the examination of coating thickness were carried out by using a S-2000 scanning electron microscope (SEM) equipped with an energy dispersion spectrometry (EDS, Evex NanoAnalysis) at an acceleration voltage of 20 kV.

A four-probe resistance measurement technique was adopted to confirm the area specific resistance (ASR) of the coated T441 steels. Prior to the ASR tests, platinum paste was coated on the both sides of the coatings and platinum meshes were also applied to establish a firm contact. Then the measurements were carried out at 800 °C in ambient air at a constant current density of 40 mA cm^{-2} by using a multimeter (Kelsey). Thus, the ASR values calculated from voltage drop could be obtained as a function of duration time. And the long-term stability of the coated samples was monitored at 800 °C up to 500 h. Details for ASR tests can be found in Ref. [16].

3. Results and discussion

Fig. 1 depicts the typical SEM images of $(Mn,Co)_3O_4$ spinel coatings precipitated by means of EPD without thermal treatment using different applied voltages. It can be clearly seen that crystalline grains with wide distribution of particle size grow on the surface of T441 steels. The average sizes of the deposited particles are estimated using the linear intercept method in SEM micrographs. It is noted that the average size of the deposit particles formed with the EPD voltage of 200 V is about 0.56 μm, and gradually increases to 0.59, 0.68 and 0.81 μm as the applied voltage ascends. It can be explained by the fact that higher applied potential exerts more pressure on particle movement. Thus, the larger particles in high field situations would easily repulse the smaller particles and occupy surface positions, which act against the packing properties of particulate film.

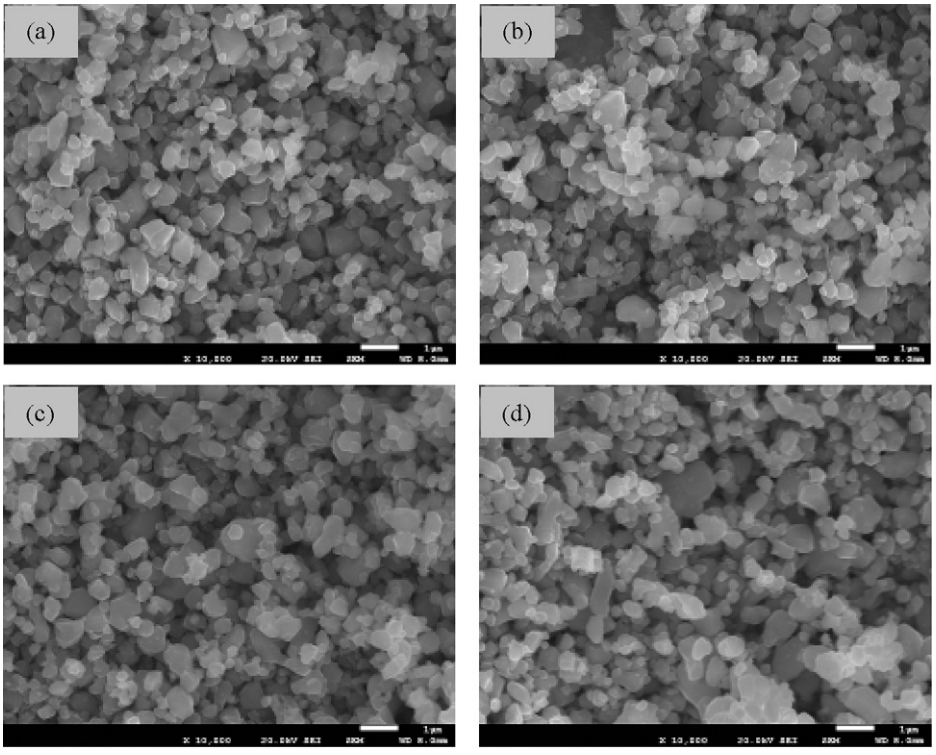

Fig. 1. SEM images of original $(Mn,Co)_3O_4$ spinel coatings without heat treatment formed under electrical field of (a) 200 V, (b) 300 V, (c) 400 V, or (d) 500 V.

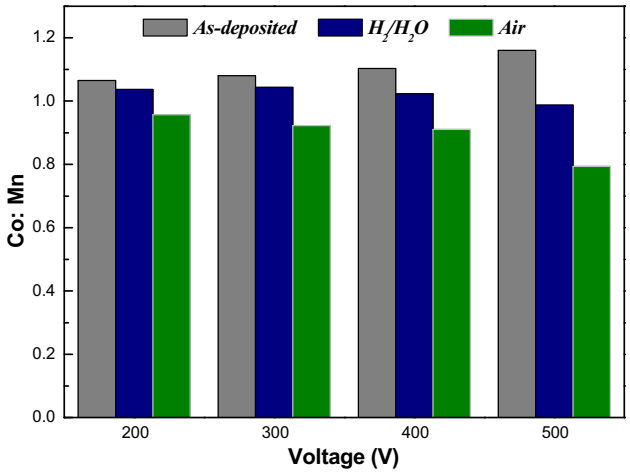

Fig. 2. The Co/Mn atomic ratios of $(Mn,Co)_3O_4$ spinel coatings before and after sintering with the change of EPD voltages and sintering atmospheres.

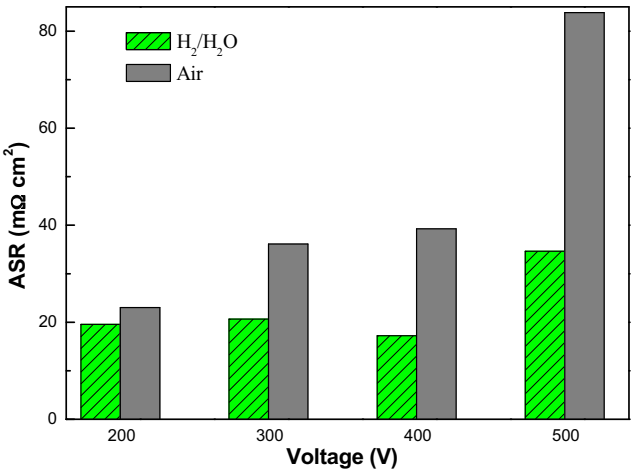

Fig. 3. The effect of applied voltage on the ASR value of the $(Mn,Co)_3O_4$ layers sintered in H_2/H_2O or air atmospheres. The measurements were performed in air at 800 °C.

The Co/Mn atomic ratios of original $(Mn,Co)_3O_4$ coatings without sintering are given in Fig. 2 as the function of applied voltage. With the increase of applied voltage, the Co/Mn atomic ratio for the initial $(Mn,Co)_3O_4$ coatings slightly increases. Combined with the fact that the formation of particulate film is only a kinetic phenomenon, it is determined that the EPD process has insignificant impact on surface composition of the coatings. In addition, the effect of sintering in H_2/H_2O or air atmospheres on the Co/Mn atomic ratios of the coatings is illustrated in Fig. 2. Compared with the originally deposited $(Mn,Co)_3O_4$ coatings, there is a drop in the Co/Mn atomic ratios after thermal treatment, especially the coatings sintered in air atmosphere. This can be attributed to the diffusion of Mn from metal substrate to the surface during sintering. It should also be noted that there is a smaller change in the Co/Mn atomic ratios among the original and sintered coatings formed with smaller deposition voltages. The Co/Mn ratios in the sintered coatings using smaller voltage than 500 V are still close to 1 owing to the proper driving force of electrical field. While at 500 V the inferior packing properties obtained at this voltage result in low surface densification and increase diffusion channels. These results imply that the spinel layers deposited with the smaller voltage than 500 V have suitable packing behavior.

Fig. 3 shows ASR values of the $(Mn,Co)_3O_4$ layers treated with different voltages and sintering atmospheres. Concerning the coatings sintered in air atmosphere, it can be observed that ASR value increases along with the augment of the applied voltage. In particular, there is a big gap in contact resistance of the coatings between electrical field of 400 V and 500 V. The ASR for the coating deposited using electrical field of 500 V achieves 83.8 $m\Omega\,cm^2$. This implies that the sintered coating with high field of 500 V cannot provide a good barrier against Mn or Cr diffusion due to low surface densification. For the coatings sintered in H_2/H_2O atmosphere, there is a small movement in ASR values until the applied voltage increases to 400 V. The ASR for the $(Mn,Co)_3O_4$ film deposited with 400 V is only 17.2 $m\Omega\,cm^2$, indicating that the deposited coating can offer high conductivity for SOFCs application. Moreover, in all cases, the ASR of the coatings sintered in H_2/H_2O shows a lower value than that in air under the same applied voltage, which indicates that the reduced sintering atmosphere results in improved conduction properties of the protection layers.

The effect of the sintering atmosphere is further compared for the $(Mn,Co)_3O_4$ spinel layers formed with electrical field of 400 V using SEM. Differences are observed concerning the surface morphology of $(Mn,Co)_3O_4$ spinel coatings sintered in H_2/H_2O and air atmospheres as shown in Fig. 4. It can be seen that the particles size of $(Mn,Co)_3O_4$ spinel coating sintered in air is obviously bigger than that in H_2/H_2O. In addition, the structure of the coating sintered in air atmosphere appears more porous suggesting that it would act as an unfavorable barrier to Cr-outward transport. The morphology for $(Mn,Co)_3O_4$ spinel film sintered in H_2/H_2O atmosphere appears to be a more compact coating. Such a continuous and dense coating would be extremely promising to protect against Cr penetration and stabilize the long-term performance of SOFC operation.

Fig. 5 represents the SEM cross-sections of the $(Mn,Co)_3O_4$ spinel coatings treated in H_2/H_2O and air atmospheres, along with EDS line scans across the surface coatings. It can be observed that the coatings are composed of Mn–Co based oxide layer and Cr based

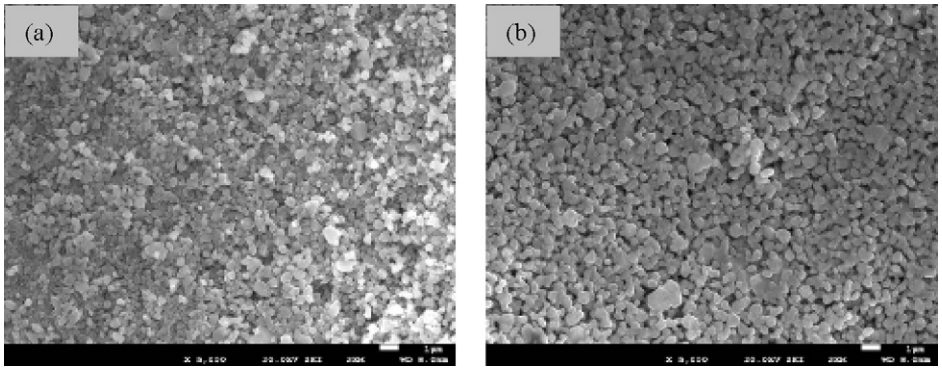

Fig. 4. SEM photographs of the $(Mn,Co)_3O_4$ coatings sintered in (a) H_2/H_2O and (b) air atmospheres.

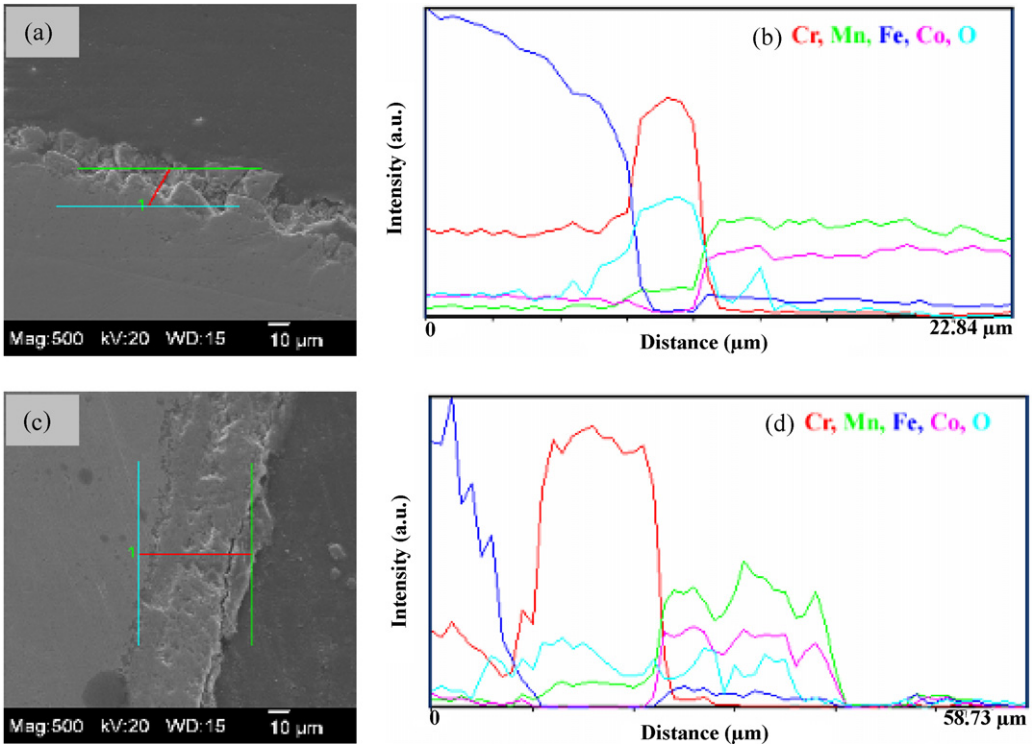

Fig. 5. (a and c) Cross-sectional SEM images, respectively, for the coatings sintered in H_2/H_2O and air atmospheres. (b and d) EDS line scans acquired on the corresponding SEM observations from (a) and (c), respectively.

oxide sublayer. And the growth of the Cr based oxide sublayers suggests oxygen transport through Mn–Co based oxides and Cr diffusion from substrate during sintering. In the case of the spinel coating sintered in air atmosphere, a Mn–Co based oxide scale of about 14.5 μm and a Cr based oxide scale of about 15.0 μm grow on the metal substrate. This demonstrates that a significant amount of Cr has migrated from substrate. For the spinel coatings sintered in H_2/H_2O atmosphere, the thicknesses of Mn–Co based oxide layer and Cr based oxide sublayer decrease to about 12.1 μm and 2.9 μm, respectively. The obvious reduction in the thickness of Cr based oxide layer may be explained in terms of the low oxygen partial pressure in the sintering gas. As a consequence, the heat treatment in H_2/H_2O atmosphere can significantly reduce the sub-coating chromia scale.

Fig. 6(a) compares XPS spectra in the Mn 2p region for the coatings sintered in H_2/H_2O and air atmospheres. Two signals in the Mn 2p region correspond to Mn $2p_{3/2}$ and Mn $2p_{1/2}$ doublet, respectively. The binding energy of Mn $2p_{3/2}$ line in MnO has been reported in the range of 640.5–641.1 eV [17–19]. Thus, the Mn $2p_{3/2}$ peak occurring at 641.0 eV for the $(Mn,Co)_3O_4$ spinel coating sintered in H_2/H_2O indicates the existence of MnO phase. The rather broad full width half maximum (FWHM) of the Mn $2p_{3/2}$ line suggests the co-existence of Mn^{2+} and Mn^{3+} species at the coating surface. Hence, the original $(Mn,Co)_3O_4$ phase is partially reduced into low-valence Mn oxides when sintering in the reduced atmosphere. For the sample sintered in air atmosphere, Mn 2p peaks shift to higher binding energy. This implies that the oxidation of Mn^{2+} ions occurs on the surface of the air-treated coating due to high oxygen partial pressure. Moreover, the presence of Mn^{4+} cannot be excluded in the sintered samples because of the typically easy formation in the Mn–Co spinel systems [20].

Deconvolution of Mn $2p_{3/2}$ peak can give useful information regarding the Mn^{2+} contents [21]. By peak deconvolution, the Mn $2p_{3/2}$ signals are fitted by subtracting the Mn^{2+} $2p_{3/2}$ and Mn^{x+} $2p_{3/2}$ electrons ($3 \le x \le 4$) on the same binding energies of 640.5 and 642.0 eV, respectively, for the two coatings. The deconvolution analyses of Mn $2p_{3/2}$ lines are illustrates for the coatings sintered in H_2/H_2O and air atmospheres in Fig. 6(b) and (c). In the terms the results of relative intensity, the Mn^{2+} species on the coatings sintered in H_2/H_2O and air atmospheres account for about 50% and 16%, respectively. Normally, there are two M^{3+} and one M^{2+} per formula unit in $(Mn,Co)_3O_4$ spinel structure. Two-thirds of Mn and Co would have a valence of 3+ to maintain charge neutrality. Thus, it further confirmed that the reduced oxides derived from H_2/H_2O atmosphere, like MnO, are embedded in the protective coating, which would favor the inhibition of premature degradation of SOFC interconnects during long-term operation.

In order to distinguish the binding energies of the Co^{2+} and Co^{3+} species, the XPS spectra in the Co 2p region recorded from the two coatings are fitted as shown in Fig. 7. All these spectra were deconvoluted into two spin–orbit doublets (Co^{2+} $2p_{3/2}$–Co^{2+} $2p_{1/2}$ and Co^{3+} $2p_{3/2}$–Co^{3+} $2p_{1/2}$) and four satellite peaks. The basic constraints include the relative intensity ratio of 1:2 for $2p_{1/2}$–$2p_{3/2}$ lines and equal width for the four satellite signals. According to the literatures [22–24] and the Gaussian/Lorentzian fitting, the binding energies of 779.5 and 794.5 eV are assigned to the Co^{3+} $2p_{3/2}$ and Co^{3+} $2p_{1/2}$ electrons, and the peak at 780.4 eV and the $2p_{3/2}$–$2p_{1/2}$ splitting of 15.2 eV are characteristic of Co^{2+} species. In addition, two satellite peaks related to the species of Co^{2+} ions ($S(Co^{2+})$) appear at about 6.2 and 8.5 eV beyond the Co^{2+} $2p_{3/2}$ and Co^{2+} $2p_{1/2}$ peaks. And there are two contributions at the binding energies of 784.4 and 800.6 eV associated with the satellite peaks ($S(Co^{3+})$) of Co^{3+} $2p_{3/2}$ and Co^{3+} $2p_{1/2}$ electrons.

The Co^{2+}/Co^{3+} ratios on the coating surfaces are obtained from the inspection of relative intensities of the above Co^{2+} and Co^{3+} contributions. It can be estimated that the Co^{2+} species occupy 81.5% and 62.4% of the total cobalt compounds for the coatings sintered in H_2/H_2O and air atmospheres, respectively. Consequently, the initial spinel phase in H_2/H_2O atmosphere is partially changed with the reduction of Mn and Co cations to lower valences, which would be

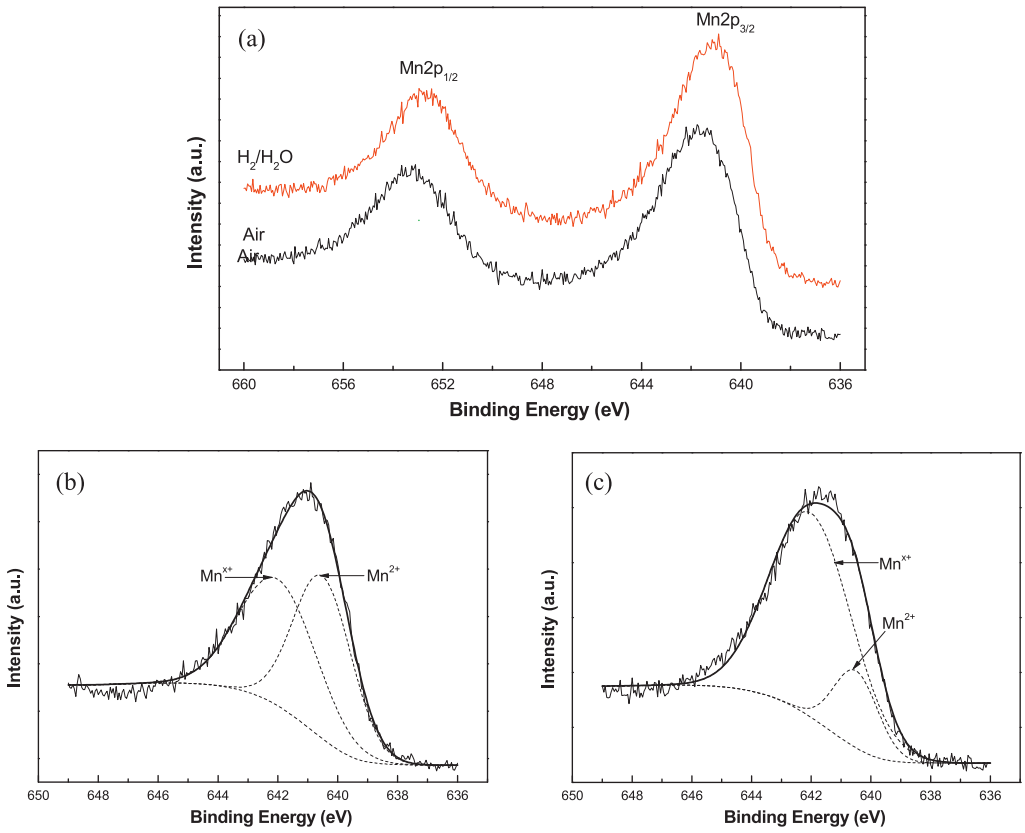

Fig. 6. Comparison of XPS spectra in Mn 2p region obtained on the coatings sintered in different atmospheres: (a) Mn 2p peaks from experiment data; fitted Mn $2p_{3/2}$ lines for (b) the H_2/H_2O-treated coating and (c) the air-treated coating.

associated with the loss of oxygen. In contrast, heat treatment in air leads to further addition of oxygen into the spinel coating. Thus, the thick Cr based oxide layer growing in the air-treated sample can be explained by the inward diffusion of excessive oxygen to interface.

The time-dependence of ASR, which was measured in air for 500 h, for the coatings sintered in H_2/H_2O and air atmospheres are compared in Fig. 8. Obviously, there is a large difference in ASR between the two coatings during oxidation, and the ASR gap steadily increases over time. Regarding the coating sintered in H_2/H_2O atmosphere, it exhibits an initially low ASR value and slight increase of ASR over the span of the test. After the oxidation of 500 h, the ASR value is around 59 $m\Omega\,cm^2$, indicating high stability and good barrier properties of the H_2/H_2O-treated coating. In comparison, the ASR of the air-treated coating starts at a relatively higher value, due to the surface microstructure resulting in relatively high contact resistance. Also, it can be observed that the resistance shows a dramatic increase over a period of time, and ends up at about 195 $m\Omega\,cm^2$ after testing of 500 h. The high ASR value can be primarily attributable to the easy diffusion of Cr from thick Cr based oxide sublayer towards the low-density surface in the air-treated coating. Moreover, the abrupt increases of resistance at some points could be related to the cracking, spalling or a detachment of the scale from the alloy substrate, suggesting the instability of the air-treated coating during long-term operation of SOFC interconnects.

On the contrary, diffusion through the coating sintered in H_2/H_2O atmosphere is much more difficult. Moreover, as more oxygen vacancies exist in the initially H_2/H_2O-treated coating due to the reduction of high-valence Mn and Co cations, the subsequent re-formation of the Spinel structure in the initial oxidation stage of ASR measurements would be expected to cause the coating to become even much denser. The oxidation reaction of reduced

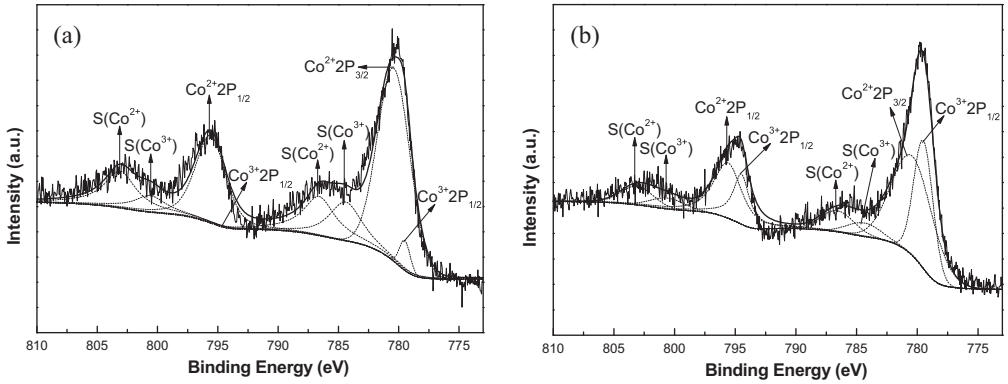

Fig. 7. XPS patterns in Co 2p region for the $(Mn,Co)_3O_4$ spinel coatings sintered in (a) H_2/H_2O and (b) air atmospheres.

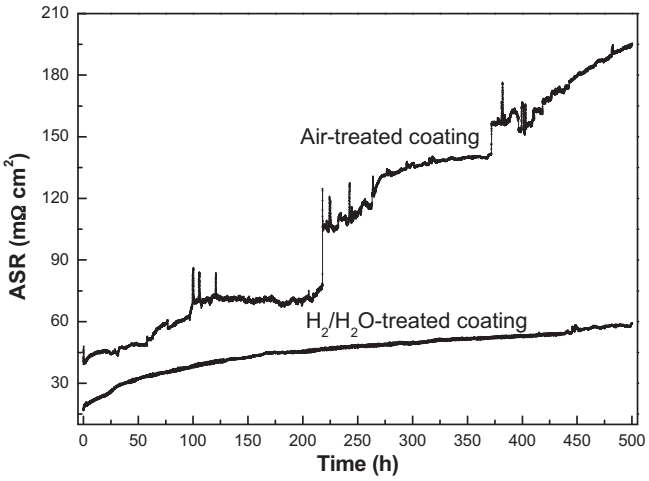

Fig. 8. ASR results of the H_2/H_2O-treated and the air-treated coatings measured in air at 800 °C.

phases would be dominant to occur during the initial oxidation stage of the H_2/H_2O-treated coating, which would inhibit the oxygen diffusion towards interface and the further growth of Cr base oxide sublayer. More importantly, a denser coating after the reformation of the Spinel phase would further reduce the diffusion rate of oxygen from air and Cr from substrate. Therefore, significant improvement in the long-term stability and electrical conductivity can be achieved for the coating fabricated by EPD followed with reduced-atmosphere sintering.

The XPS patterns for the detailed scans of Mn 2p and Cr 2p regions are investigated using the H_2/H_2O-treated and air-treated coatings after oxidation of 500 h at 800 °C in air. As shown in Fig. 9(a), there is no obvious difference in the positions of the Mn 2p peaks for the two coatings after oxidation. The binding energy of

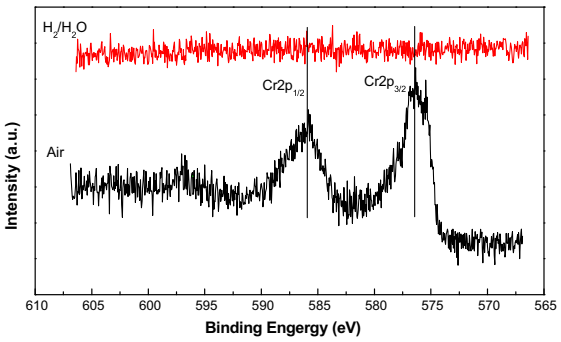

Fig. 10. Comparison of XPS patterns in Cr 2p region acquired on the H_2/H_2O-treated and air-treated coatings after oxidation of 500 h in air at 800 °C.

Mn $2p_{3/2}$ for the two samples is about 641.8 eV and the spin orbital splitting is 11.7 eV, which is in good agreement with reported values for MnO_2 [25]. Also, it is reasonable to assume from the wide Mn $2p_{3/2}$ peaks that Mn^{3+} and Mn^{4+} species co-exist at the coating surfaces after oxidation duration of 500 h.

Inspections of fitted Mn $2p_{3/2}$ peaks (see Fig. 9(b) and (c)) show Mn^{3+}/Mn^{4+} ratios for the H_2/H_2O-treated and air-treated coatings are around 2:1 and 1:1, respectively. It is evident that the occupied proportion of lower valence Mn species in the H_2/H_2O-treated coating after oxidation of 500 h is larger than that in air-treated sample. Thus, the long-term performance of the H_2/H_2O-treated sample can be well maintained due partially to the lower degree of oxidation. Moreover, no Cr 2p peaks are observed from the detailed scan of XPS patterns after oxidation duration of 500 h, as shown in Fig. 10. This can be ascribed to thin Cr based oxide sublayer, low diffusion rate of Cr from metal substrate and dense Mn–Co based oxide layer obtained for the H_2/H_2O-treated sample. Unlike the H_2/H_2O-treated sample, the Cr 2p peaks obviously occur at the surface of the air-treated sample after 500 h, indicating that Cr penetrates into

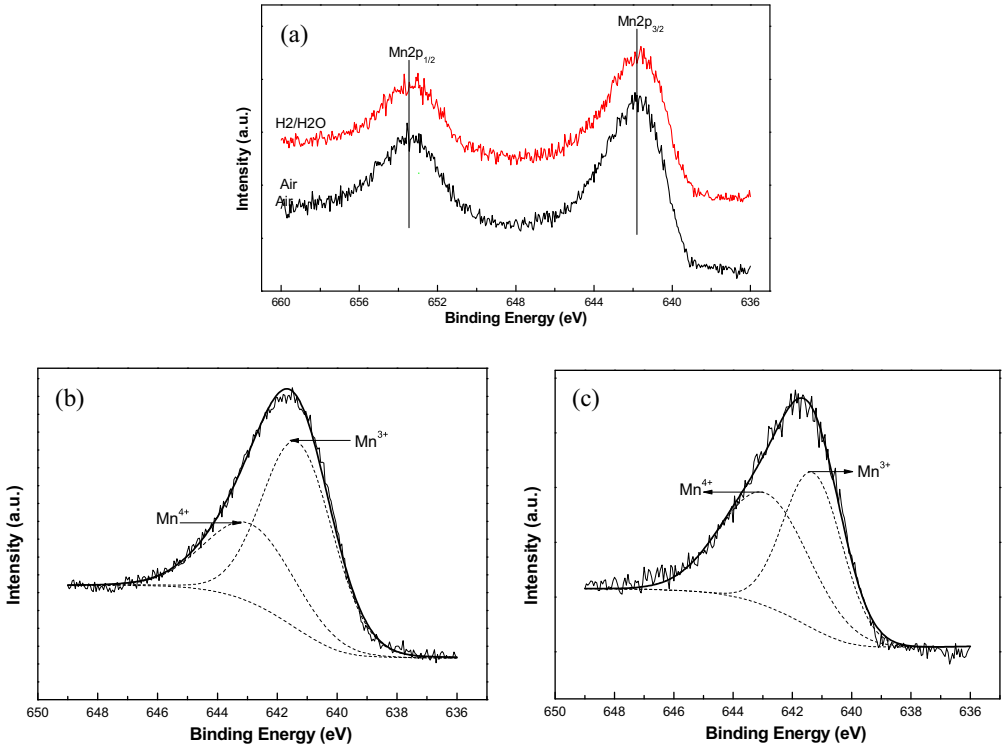

Fig. 9. XPS patterns in Mn 2p region for the H_2/H_2O-treated and air-treated coatings after oxidation of 500 h in air at 800 °C: (a) Mn 2p signals obtained from experiment data, (b) fitted Mn $2p_{3/2}$ peaks of (b) the H_2/H_2O-treated coating and (c) the air-treated coating.

the surface. The existence of Cr species after 500 h explains the obvious reduction of electrical conductivity. Therefore this work suggests that the electrophoretically deposited spinel coating sintered in H_2/H_2O atmosphere can meet the requirements for SOFC interconnects.

4. Conclusions

EPD followed by reduced-atmosphere sintering appears to provide a good approach for fabricating protective layers of the $(Mn,Co)_3O_4$ spinel onto the Cr-containing steel interconnects. EPD voltages and sintering atmospheres are found to have a significant influence on microstructure, composition and electrical conductivity. In particular, long-term stability of the spinel coatings is strongly dependent on the sintering atmospheres. It is confirmed that the uniform distribution and high conductivity of the $(Mn,Co)_3O_4$ spinel coatings can be achieved by using the deposited voltage of 400 V due to the appropriate driving force of electrical field. Compared with the air-treated coating, the interfacial layer of Cr based oxide is obviously thinner for the spinel coating sintered in H_2/H_2O atmosphere due to the low oxygen partial pressure. ASR tests indicate that the H_2/H_2O-treated coating has lower resistance value and much better long-term performance than the air-treated coating. The slow increase of ASR from about 17.2 $m\Omega\,cm^2$ in an initial stage to 59 $m\Omega\,cm^2$ after oxidation of 500 h is observed for the spinel coating sintered in H_2/H_2O atmosphere. Furthermore, no Cr penetration is observed on the coating surface after long-term oxidation. The great contributions to electrical conductivity and long-term properties should be mainly attributed to thin sublayer of Cr based oxide, the surface layer with high densification and relatively low degree of oxidation.

Acknowledgements

The authors would like to thank Dr. Z. Gary Yang from PNNL for providing $(Mn,Co)_3O_4$ spinel powders and Dr. Chris Johnson for continuous encouragement and insightful technical discussion over the years. Z. Zhan acknowledges the financial support form China Scholarship Council for his visit to WVU.

References

[1] Z. Yang, G. Xia, P. Singh, J.W. Stevenson, J. Power Sources 155 (2006) 246–252.
[2] N. Shaigan, W. Qu, D.G. Ivey, W. Chen, J. Power Sources 195 (2010) 1529–1542.
[3] X. Sun, W.N. Liu, E. Stephens, M.A. Khaleel, J. Power Sources 176 (2008) 167–174.
[4] S.-S. Pyo, S.-B. Lee, T.-H. Lim, R.-H. Song, D.-R. Shin, S.-H. Hyun, Y.-S. Yoo, Int. J. Hydrogen Energy 36 (2011) 1868–1881.
[5] Y. Li, J. Wu, C. Johnson, R. Gemmen, X. Mao Scott, X. Liu, Int. J. Hydrogen Energy 34 (2009) 1489–1496.
[6] J. Wu, C.D. Johnson, Y. Jiang, R.S. Gemmen, X. Liu, Electrochim. Acta 54 (2008) 793–800.
[7] C.C. Mardare, H. Asteman, M. Spiegel, A. Savan, A. Ludwig, Appl. Surf. Sci. 255 (2008) 1850–1859.
[8] M. Reza Bateni, P. Wei, X. Deng, A. Petric, Surf. Coat. Technol. 201 (2007) 4677–4684.
[9] W.N. Liu, X. Sun, E. Stephens, M.A. Khaleel, J. Power Sources 189 (2009) 1044–1050.
[10] K. Manoj, M.K. Lu, X. Liu, J. Wu, Int. J. Hydrogen Energy 35 (2010) 7945–7956.
[11] H. Kurokawa, C.P. Jacobson, L.C. DeJonghe, S.J. Visco, Solid State Ionics 178 (2007) 287–296.
[12] Z.G. Yang, G.G. Xia, X.H. Li, J.W. Stevenson, Int. J. Hydrogen Energy 32 (16) (2007) 3648–3654.
[13] J. Wu, C.D. Johnson, R.S. Gemmen, X. Liu, J. Power Sources 189 (2009) 1106–1113.
[14] L. Besra, M. Liu, Prog. Mater. Sci. 52 (2007) 1–61.
[15] J. Yoo, S.-K. Woo, J.H. Yu, S. Lee, G.W. Park, Int. J. Hydrogen Energy 34 (2009) 1542–1547.
[16] J. Wu, C. Li, C. Johnson, X. Liu, J. Power Sources 175 (2008) 833–840.
[17] M. Fujiwara, T. Matsushita, S. Ikeda, J. Electron Spectrosc. Relat. Phenom. 74 (1995) 201–206.
[18] C. Colmenares, S. Deutsch, C. Evans, A.J. Nelson, L.J. Terminello, J.G. Reynolds, J.W. Roos, I.L. Smith, Appl. Surf. Sci. 151 (1999) 189–202.
[19] J.F. Moulder, W.F. Stickle, P.E. Sobol, K.D. Bomben, Handbook of X-ray Photoelectron Spectroscopy, ULAC-PHI, Inc., Japan, 1995.
[20] G.V. Bazuev, A.V. Korolyov, J. Magn. Magn. Mater. 320 (2008) 2267–2268.
[21] M.V. Bukhtiyarova, A.S. Ivanova, L.M. Plyasova, G.S. Litvak, V.A. Rogov, V.V. Kaichev, E.M. Slavinskaya, P.A. Kuznetsov, I.A. Polukhina, Appl. Catal. A: Gen. 357 (2009) 193–205.
[22] J.L. Gautier, E. Ríos, M. Gracia, J.F. Marco, J.R. Gancedo, Thin Solid Films 311 (1997) 51–57.
[23] A. Restovic, E. Ríos, S. Barbato, J. Ortiz, J.L. Gautier, J. Electroanal. Chem. 522 (2002) 141–151.
[24] S. Wang, B. Zhang, C. Zhao, S. Li, M. Zhang, L. Yan, Appl. Surf. Sci. 257 (2011) 3358–3362.
[25] S. Todorova, H. Kolev, J.P. Holgado, G. Kadinov, Ch. Bonev, R. Pereñíguez, A. Caballero, Appl. Catal. B: Environ. 94 (2010) 46–54.